Nanocubic Cobalt-containing Prussian Blue Analogue Derived Carbon Coated CoFe Alloy Nanoparticles for Noninvasive Uric Acid Sensing

Yunting Qin[a], Yanxue Xu[b]*, Xilan Gao[c], Xicui Zhang[d]* and Dan Xiao[b,e]*

[a]*School of Pharmacy, Chengdu University, No. 2025, Chengluo Avenue, Chengdu, P. R. China*

[b]*Institute of Advanced Study, Chengdu University, No. 2025, Chengluo Avenue, Chengdu, P. R. China*

[c]*College of Food and Bioengineering, Chengdu University, No. 2025, Chengluo Avenue, Chengdu, P. R. China*

[d]*Sichuan Institute of Product Quality Supervision & Inspection, No. 16, Xinmao Street Chengdu, China*

[e]*College of Chemical Engineering, Sichuan University, No. 29 Wangjiang Road, Chengdu, P. R. China*

Corresponding Author E-mail: xuyanxue@cdu.edu.cn; zhangxicui216@163.com; xiaodan@scu.edu.cn

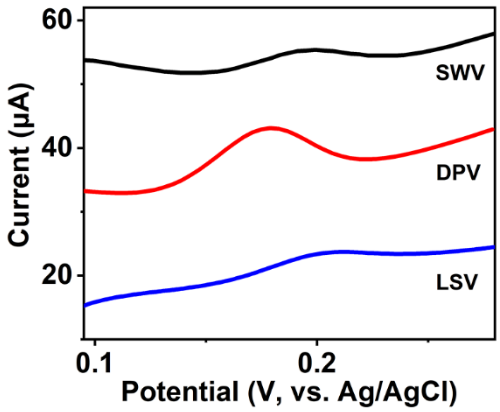

Fig. S1 The electrochemical responses of $CCF_{1.5}$/SPCE toward 5 μM UA via the method of SWV, DPV and LSV, respectively.

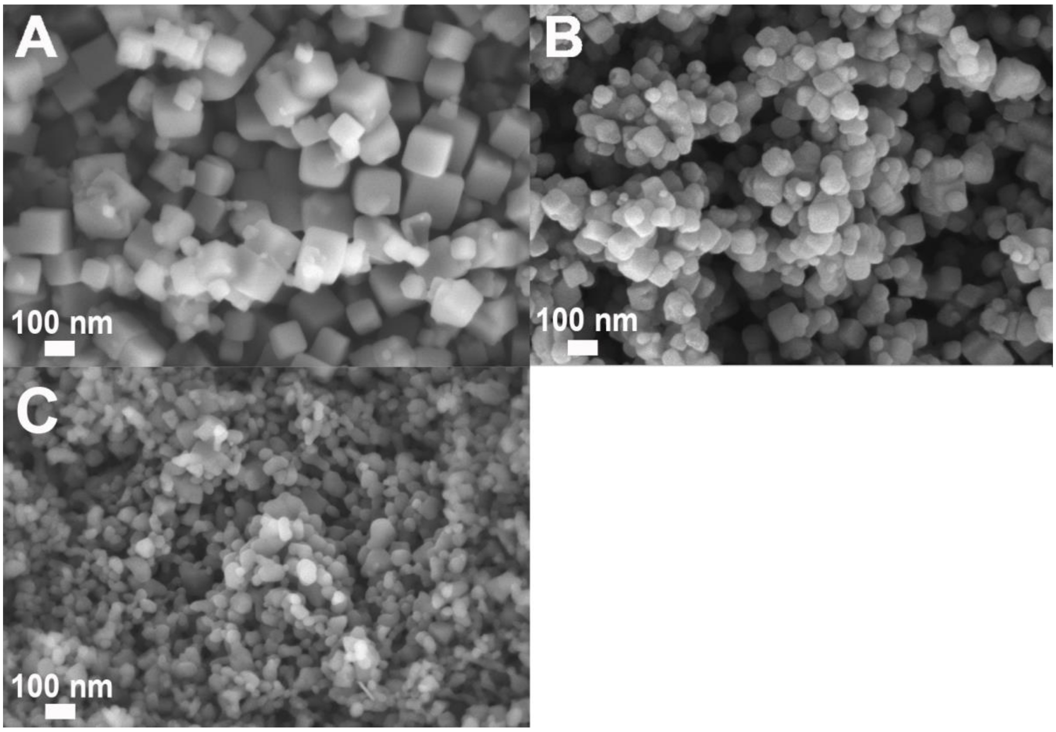

Fig. S2 SEM images of PCFs before calcination: (A) $PCF_{0.8,0}$; (B) $PCF_{1.5,0}$; (C) $PCF_{1.8,0}$.

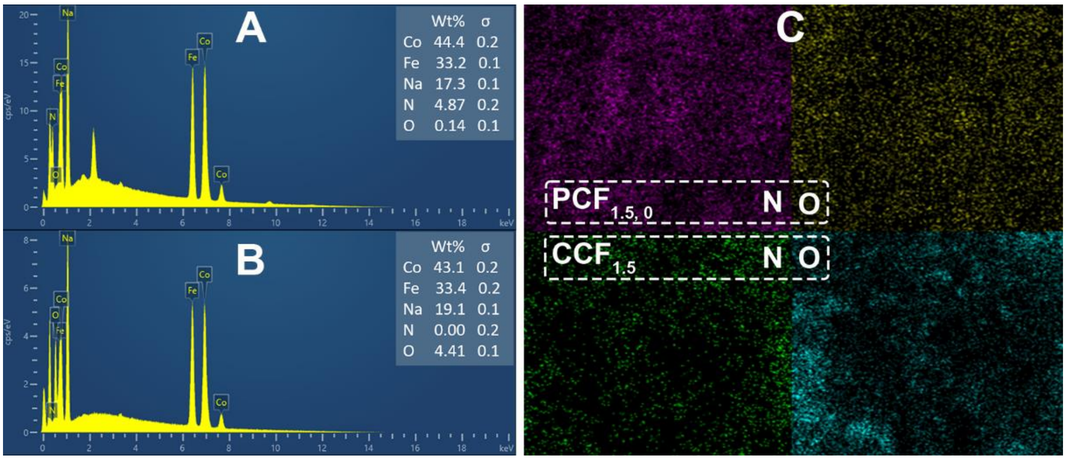

Fig. S3 Total energy dispersive spectroscopy of $PCF_{1.5,0}$ (A) and $CCF_{1.5}$ (B); N, O mapping in $PCF_{1.5,0}$ and $CCF_{1.5}$ (C).

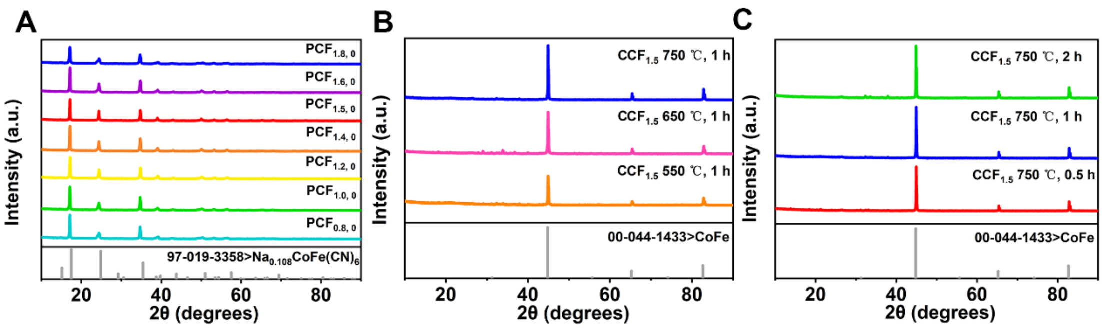

Fig. S4 (A) XRD patterns of PCFs with different initial Fe/Co ratio; (B) XRD patterns of CCFs calcined for 1 h at different temperature:550 °C, 650 °C and 750 °C, respectively; (C) XRD patterns of CCFs calcined at 750 °C for different time: 0.5 h, 1 h and 2 h, respectively.

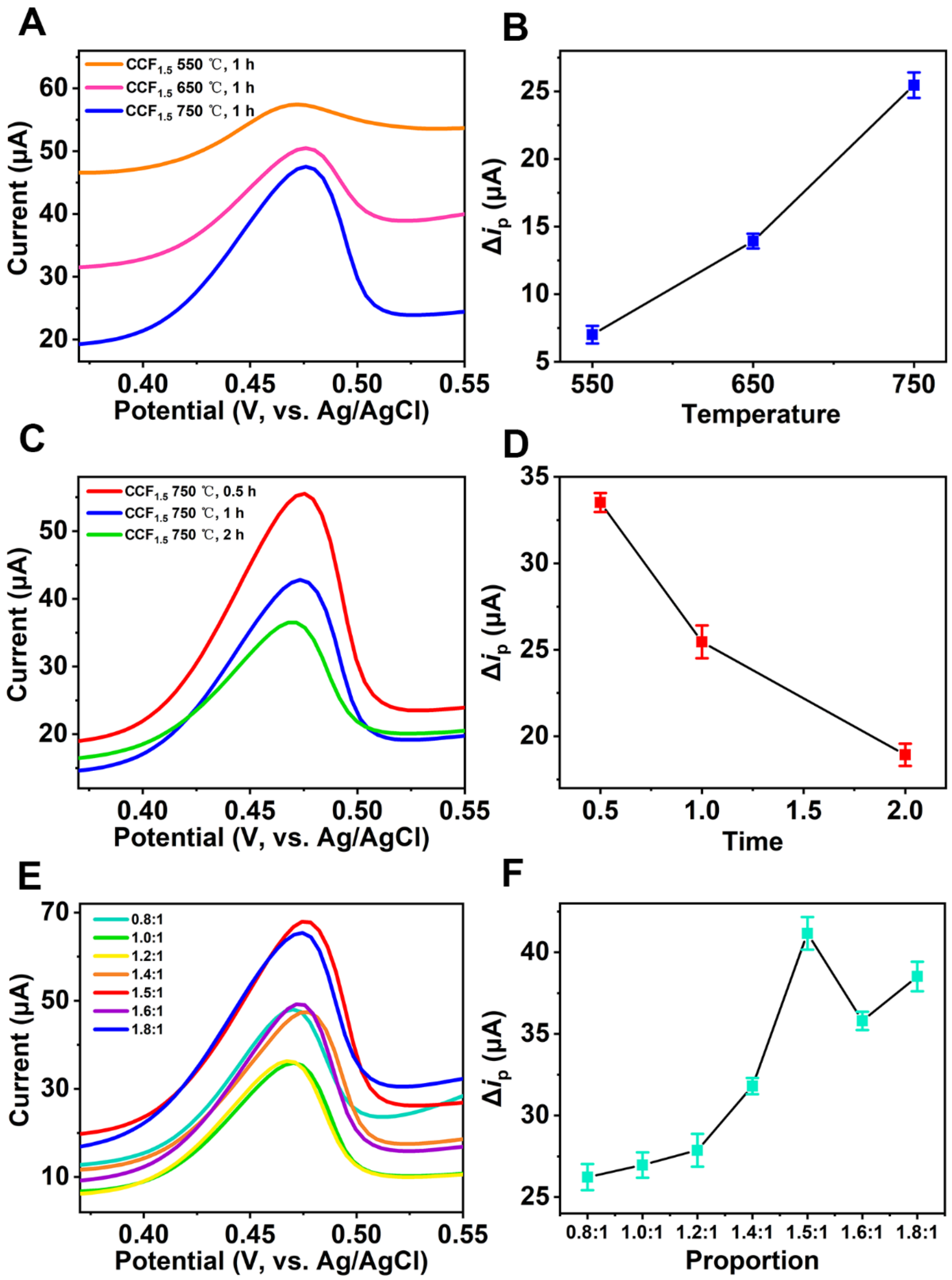

Fig. S5 DPV curves and the corresponding peak currents recorded in PBS (pH 7.0) containing 10 μM UA: (A, B) CCFs calcined for 1 h at 550 °C, 650 °C and 750 °C. (C, D) CCFs calcined at 750 °C for 0.5 h, 1 h and 2 h. (E, F) CCFs with different initial Co/Fe ratio in PCFs calcined at 750 °C for 1 h.

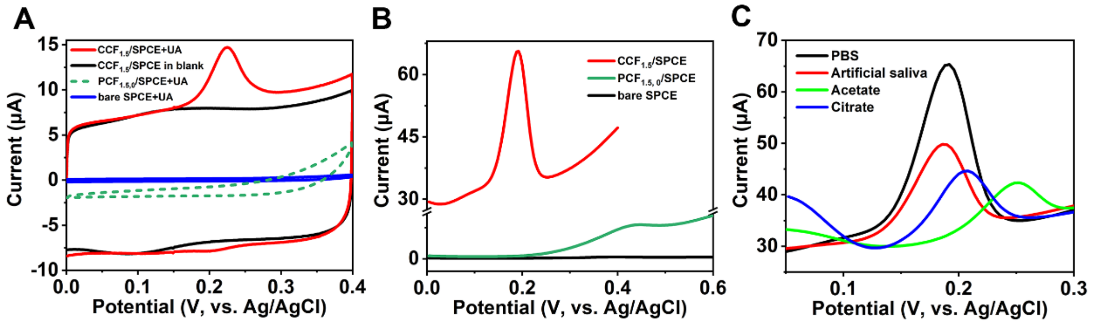

Fig. S6 (A) CV curves of bare SPCE, $PCF_{1.5,0}$/SPCE and $CCF_{1.5}$/SPCE in PBS (pH 7.0) containing 10 μM UA at the scan rate of 50 mV/s. (B) DPV curves of bare SPCE, $PCF_{1.5,0}$/SPCE and $CCF_{1.5}$/SPCE in PBS (pH 7.0) containing 10 μM UA. (C) DPV curves of $CCF_{1.5}$/SPCE in PBS, artificial saliva, acetate (pH 5.5) and citrate (pH 6.5) containing 10 μM UA.

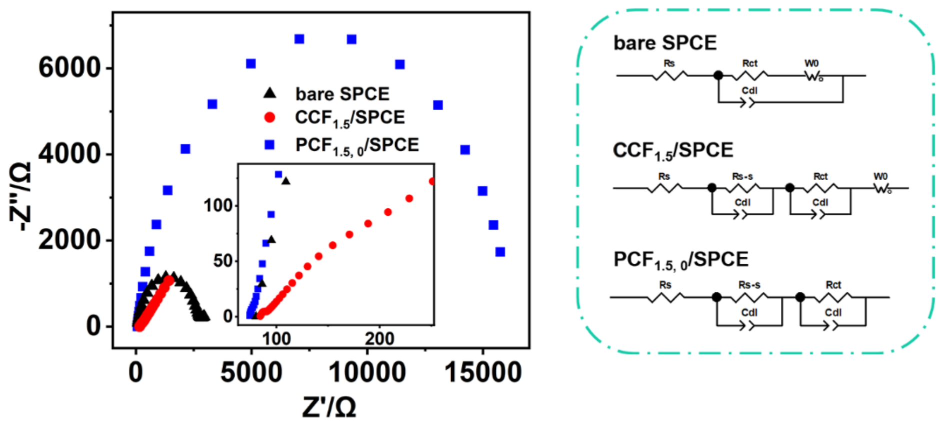

Fig. S7 EIS and the corresponding equivalent circuit diagrams of SPCE, $PCF_{1.5,0}$/SPCE and $CCF_{1.5}$/SPCE in 5 mM $[Fe(CN)_6]^{3-/4-}$ solution with 0.1 M KCl at open circuit potential.

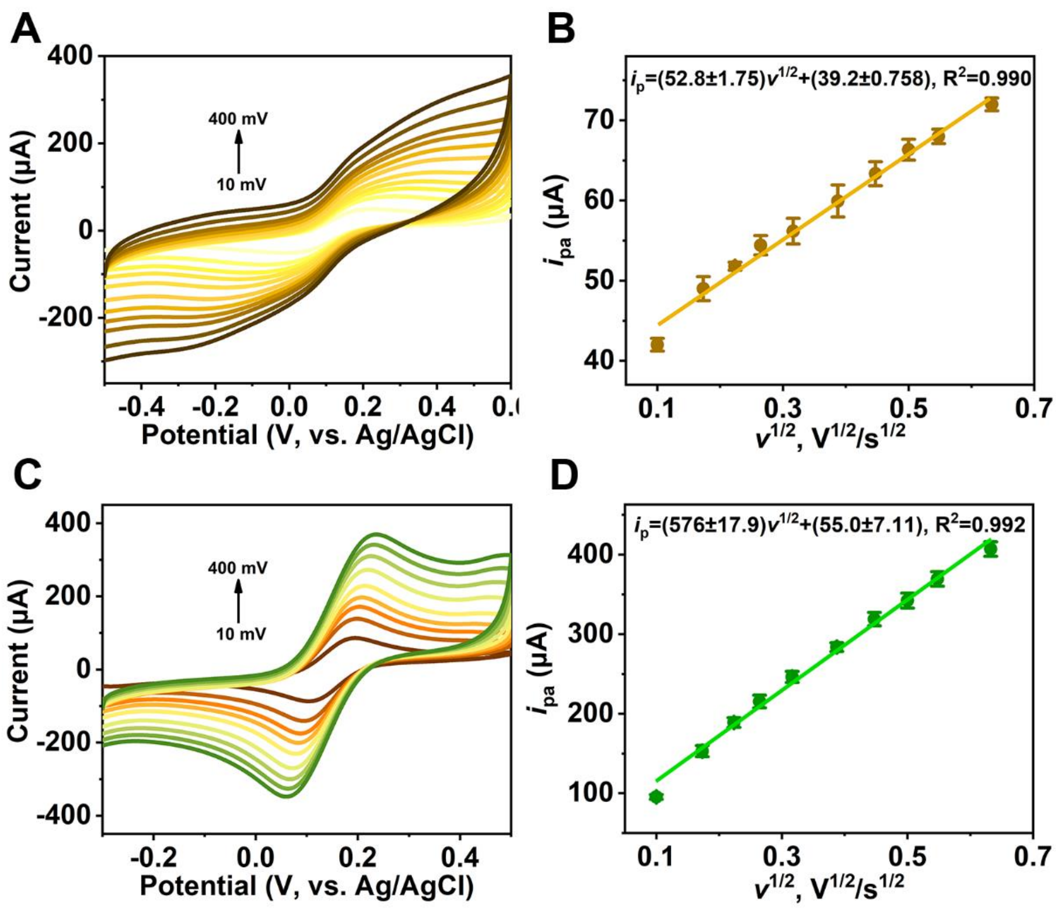

Fig. S8 CV curves and the corresponding i_{pa}~$v^{1/2}$ plots of $PCF_{1.5,0}$/SPCE (A, B) and $CCF_{1.5}$/SPCE. (C, D) in 5 mM $[Fe(CN)_6]^{3-/4-}$. The scan rate increased from 10 mV/s to 400 mV/s.

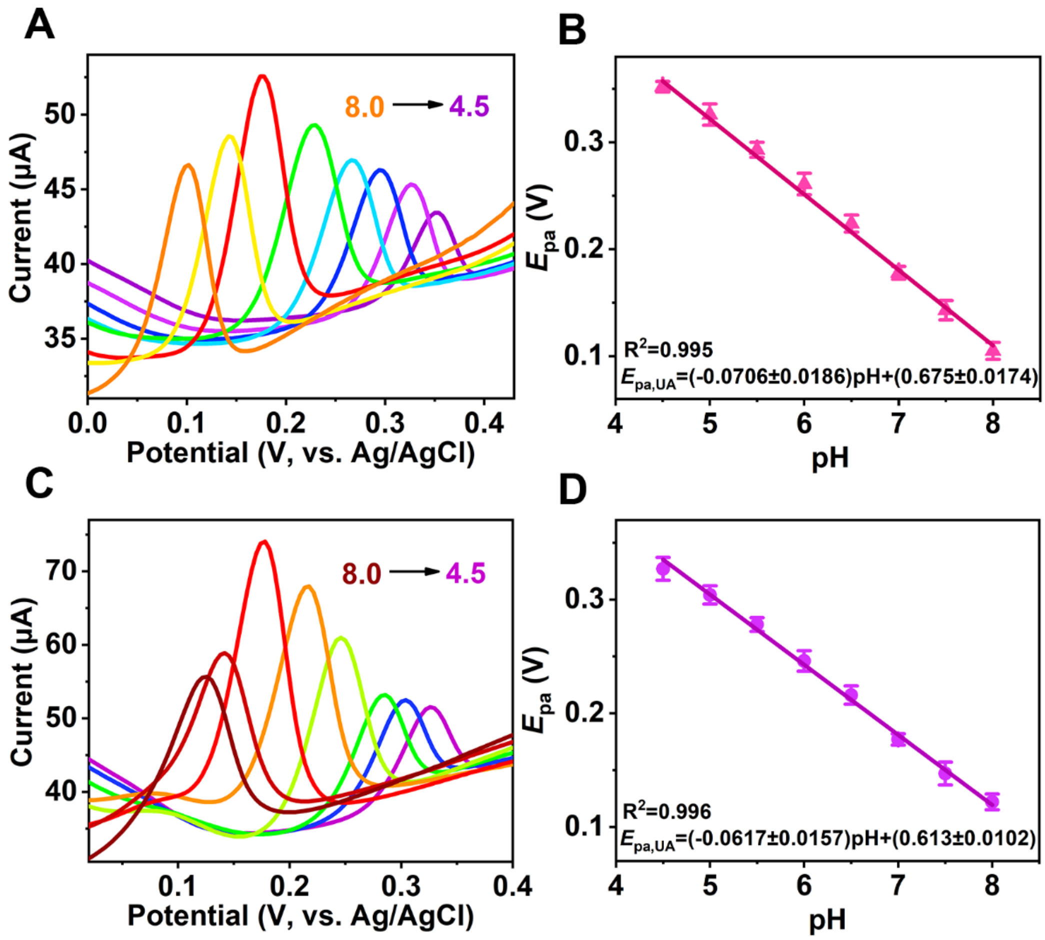

Fig. S9 pH investigation of the supporting electrolyte: DPV curves of UA (10 μM) in artificial saliva (A) and the linear fitting plots (B) of E_{pa} vs. pH values; DPV curves of UA (10 μM) in PBS (C) and the linear fitting plots (D) of E_{pa} vs. pH values.

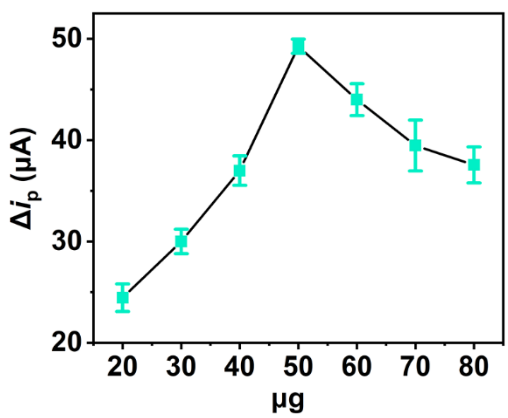

Fig. S10 Optimization of immobilized mass via DPV: Anodic peak current ($\triangle i_{pa}$) of UA on $CCF_{1.5}$/SPCEs immobilized with different mass of $CCF_{1.5}$.

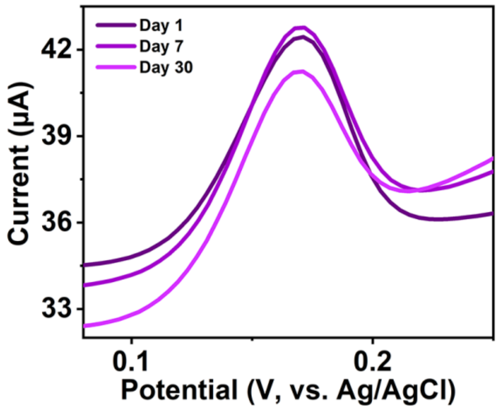

Fig. S11 Stability studies via DPV: $CCF_{1.5}$ stored with different time of 1, 7, 30 days and immobilized on SPCE responding to 5 μM UA.

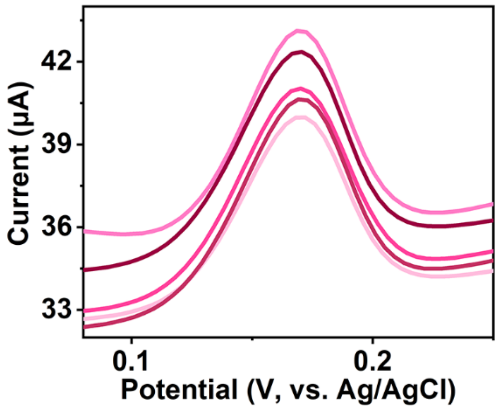

Fig. S12 Reproducibility studies via DPV: 5 different $CCF_{1.5}$/SPCEs responding to 5 μM UA

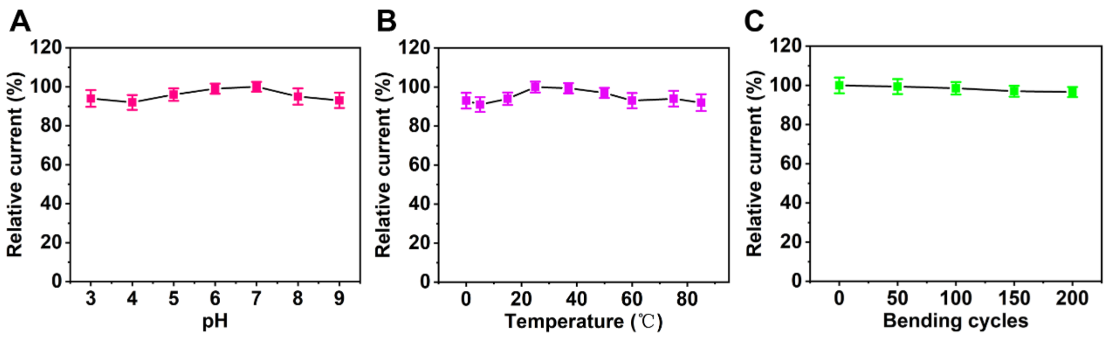

Fig. S13 Robustness studies: (A) $CCF_{1.5}$/SPCE soaked in harsh pH before testing; (B) $CCF_{1.5}$/SPCE thermal treated with different temperature; (C) $CCF_{1.5}$/SPCE bended with different bending time.

Table S1 RSD values for the reproducibility study of the five $CCF_{1.5}$/SPCEs.

	RSD[a] (%)	RSD[b] (%)
1	3.21	
2	2.63	
3	2.95	3.42
4	2.08	
5	3.15	

a. RSD for the three replicates of single electrode;

b. RSD for five electrodes

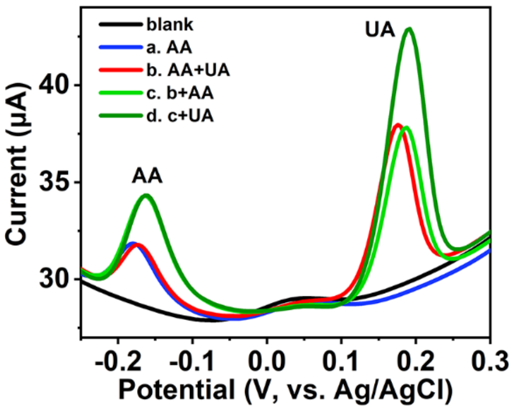

Fig. S14 Interference study of UA (5 μM) against with high concentration of AA (0.5 mM) via DPV. The addition sequence was from curve a to curve d: a. 0.5 mM AA; b. UA was added; c. AA was added based on b; d. UA was added again based on c.

Table S2 $CCF_{1.5}$/SPCE compared with the reported sensors.

Sensors	Linear range (μM)	LOD (μM)	Sample	Method	Ref.
SPE-AuNps[1]	20-200	14.64	artificial saliva	AMP	18
β-CD/CPE[2]	10-170	4.6	saliva	A	51
UOx–GO/PANI/Nf–Gr/Pt[3]	3-300	3	saliva	A	52
Uricase/PB/SPE[4]	50-1000	--	saliva and artificial saliva	CA	53
CME[5]	--	20	saliva	CV	54
Uricase/MWCNTs/SPE[6]	5-1000	0.33	saliva	CA	55
α-$Ni_{0.75}Zn_{0.25}(OH)_2$/SPE[7]	100-1400	0.023	saliva and artificial saliva	CV	56
PEDOT–GO/ITO/PAD[8]	2-1000	0.75	saliva and artificial saliva	DPV	57
3D-printed G-PLA sensor[9]	0.5-250	0.02	saliva and artificial saliva	DPV/ BIA-MPA	58
CVE_{act}[10]	0.09-700	0.05	saliva and artificial saliva	LSV	59
Co_3O_4–ERGO/SPE[11]	5-500	1.5	saliva	DPV	60
BSAT/LIG[12]	20-1000	2.1	saliva	DPV	61
$CCF_{1.5}$/SPCE	0.04-30	0.0153	saliva	DPV	This work

A-amperometry
CA-chronoamperometry
BIA-MPA-multiple-pulse amperometry combined with batch-injection analysis
AMP-amperometric reader AMP3291
LSV-linear sweep voltammetry

1. screen printed electrode-gold nanoparticles
2. β-cyclodextrin/carbon paste electrode
3. uricase-Graphene oxide/polyaniline/Nafion-graphene/Pt electrodes
4. Uricase/Prussian Blue/screen printed electrode
5. carbon microdisc electrode
6. Uricase/Multi-walled carbon nanotubes/screen printed electrode
7. α-$Ni_{0.75}Zn_{0.25}(OH)_2$/screen printed electrode
8. poly (3,4-ethylenedioxythipohene)-graphene oxide/indium tin oxide/Paper-based analytical devices
9. 3D-printed polylactic acid containing graphene sensor
10. carbon veil electrode activated at 2.0 V;
11. Co_3O_4-reduced graphene oxide/screen printed electrode
12. bovine serum albumin and Tween-20/Laser-induced graphene electrode

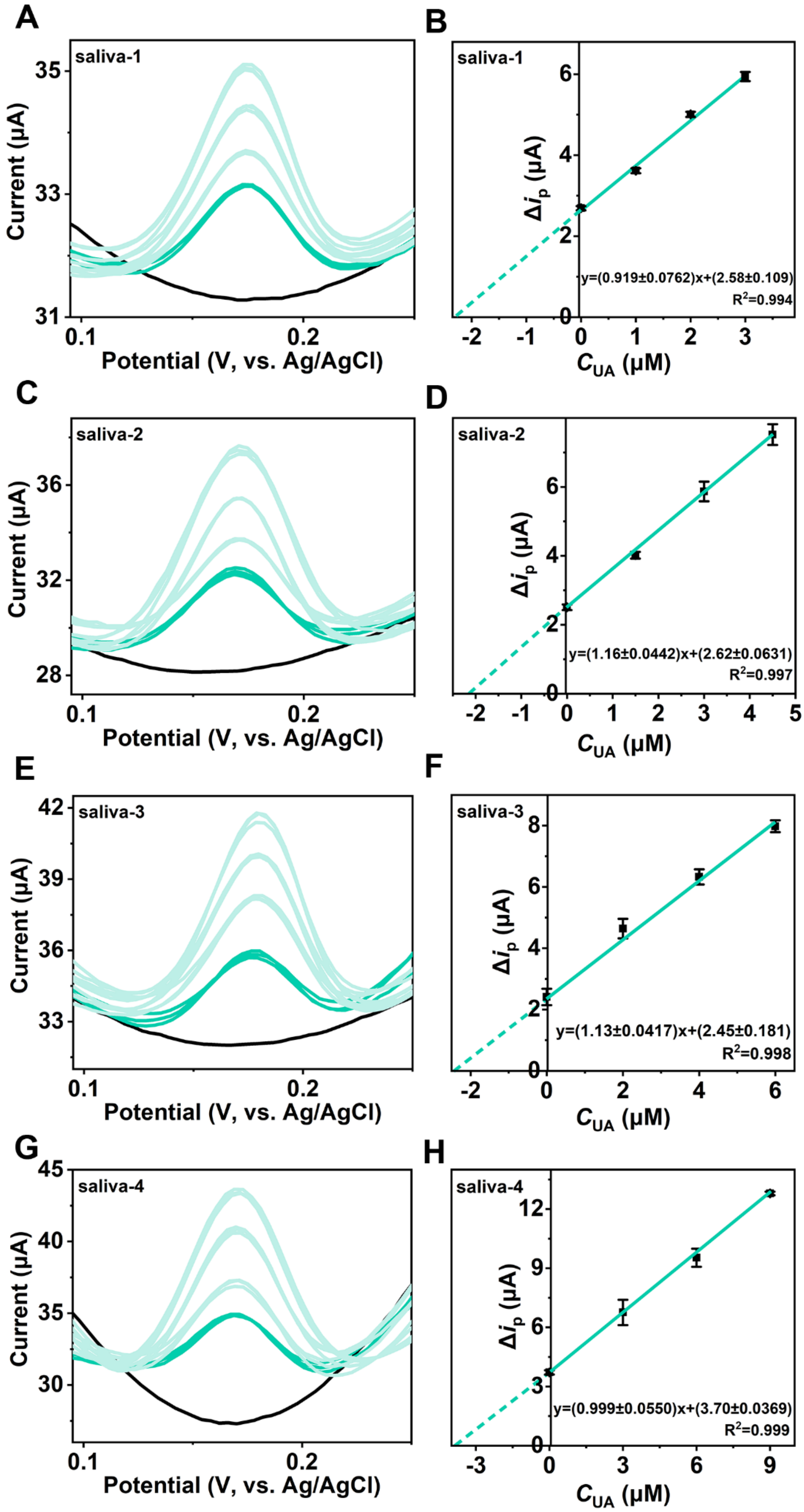
A
saliva-1
Current (μA)
Potential (V, vs. Ag/AgCl)
B
saliva-1
Δi_p (μA)
y=(0.919±0.0762)x+(2.58±0.109)
R²=0.994
C_UA (μM)
C
saliva-2
Current (μA)
Potential (V, vs. Ag/AgCl)
D
saliva-2
Δi_p (μA)
y=(1.16±0.0442)x+(2.62±0.0631)
R²=0.997
C_UA (μM)
E
saliva-3
Current (μA)
Potential (V, vs. Ag/AgCl)
F
saliva-3
Δi_p (μA)
y=(1.13±0.0417)x+(2.45±0.181)
R²=0.998
C_UA (μM)
G
saliva-4
Current (μA)
Potential (V, vs. Ag/AgCl)
H
saliva-4
Δi_p (μA)
y=(0.999±0.0550)x+(3.70±0.0369)
R²=0.999
C_UA (μM)

Fig. S15 Determination of UA in four saliva samples (saliva-1, saliva-2, saliva-3, saliva-4) with $CCF_{1.5}$/SPCE: A known amount of saliva sample was added in artificial saliva (pH 7.0) (green curves) and a series of standard solution of UA were added successively (light green curves). The added volume for saliva-1, saliva-2, saliva-3, saliva-4 was 100, 150, 200 and 300 μL, respectively. The total volume of background electrolyte was maintained as 10 mL.

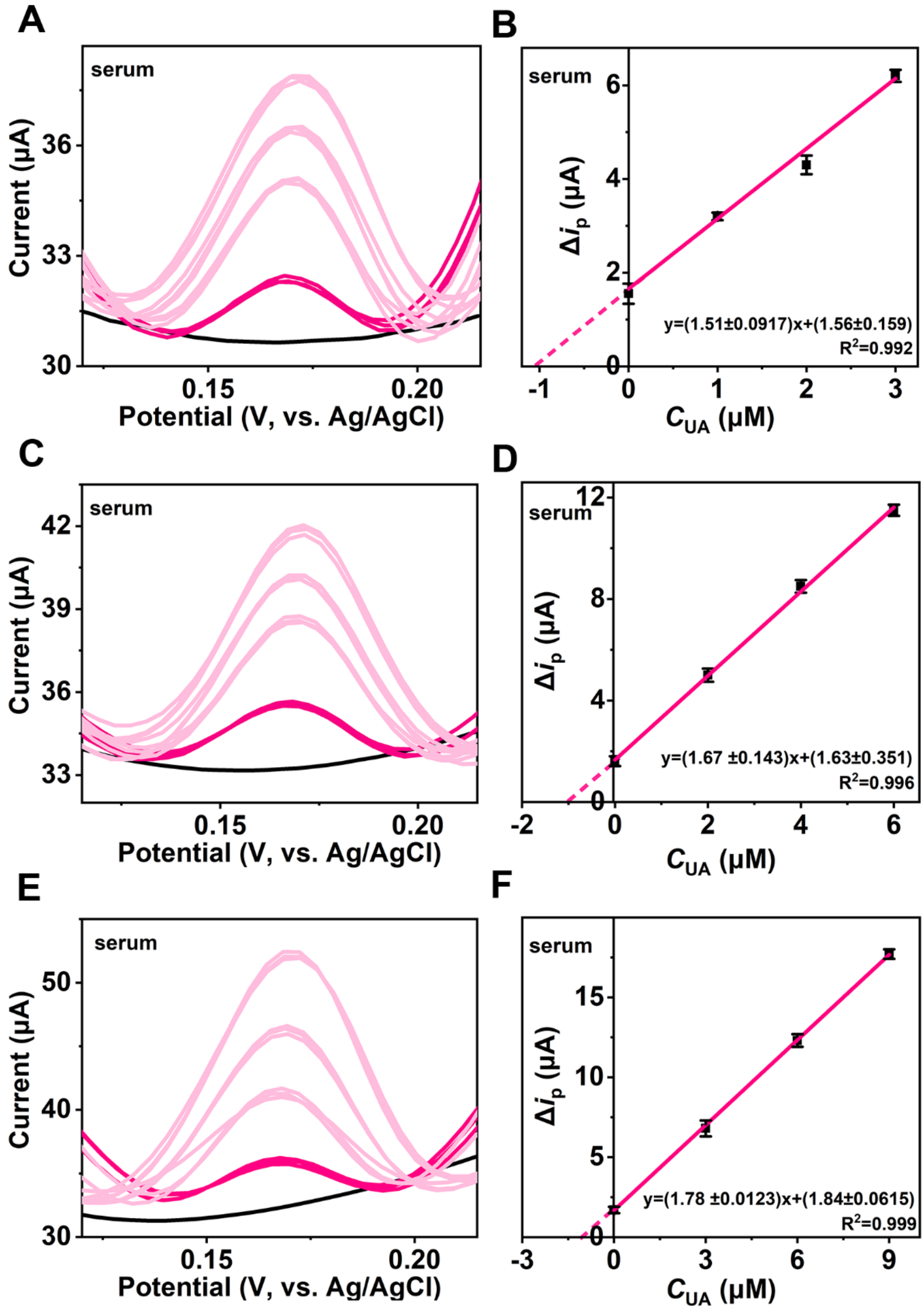

Fig. S16 Determination of UA in serum with $CCF_{1.5}$/SPCE for three replicates: 50 μL serum was added in 9.95 mL PBS (pH 7.0) (pink curves) and a series of standard solution of UA were added successively (light pink curves). The total volume of background electrolyte was maintained as 10 mL.

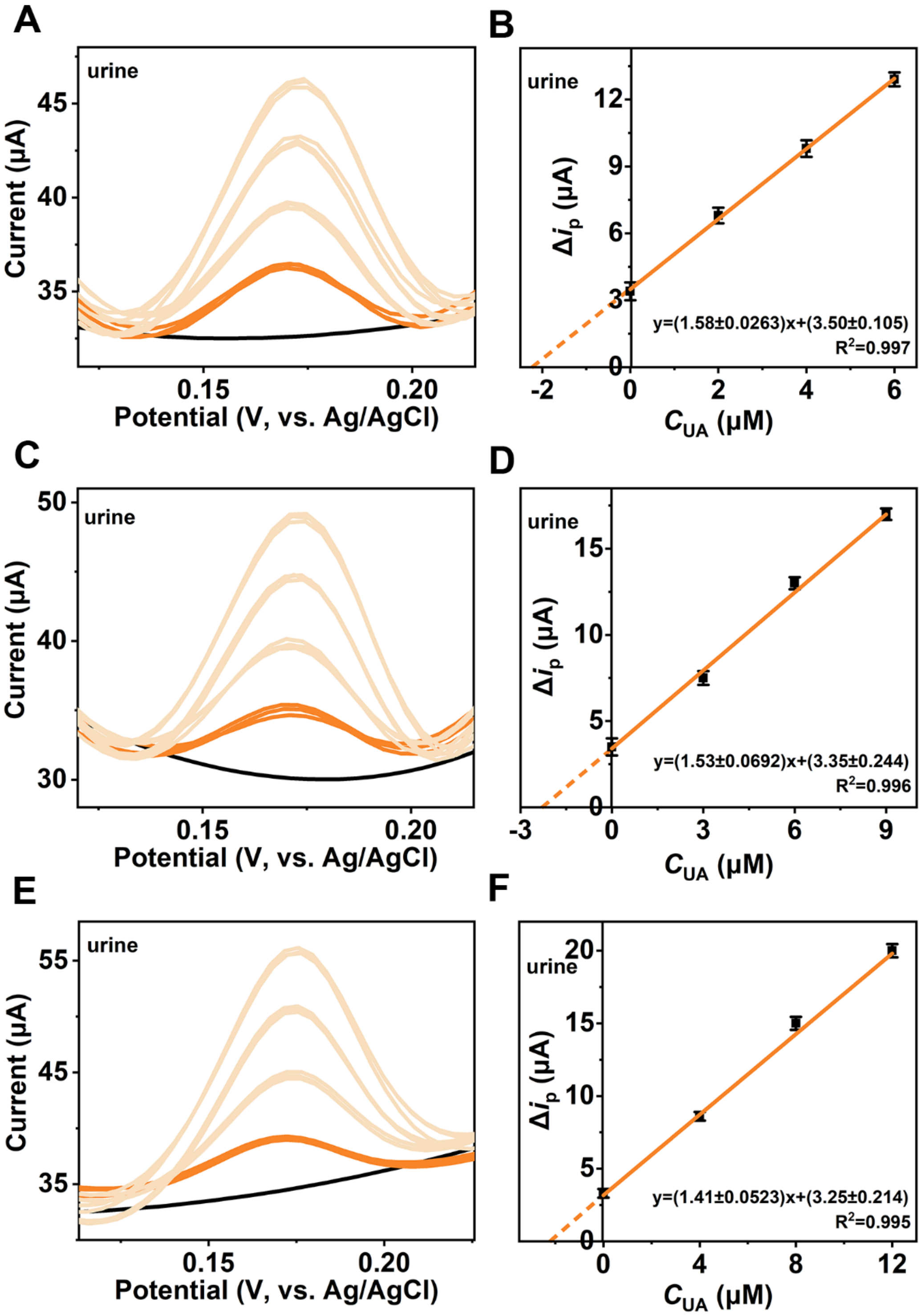

Fig. S17 Determination of UA in urine with $CCF_{1.5}$/SPCE for three replicates: A known amount of urine sample was added in PBS (pH 7.0) (orange curves) and a series of standard solution of UA were added successively (light orange curves). The added volume for urine was 10 μL. The total volume of background electrolyte was maintained as 10 mL.

Table S3 Determination and recoveries of UA in serum and urine.

Samples	Found[a]	AVG (±RSD)	Add (μM)	Found[b] (μM)	Recovery (%)	RSD (%)
UA in serum	206 μM	206 (±1.71) μM	1.0	1.03	103	2.02
	202 μM		2.0	1.98	99.3	
	209 μM		3.0	2.99	99.7	
UA in urine	2.22 mM	2.24 (±2.54) mM	2.0	2.04	102	3.01
	2.19 mM		3.0	2.94	98.0	
	2.30 mM		4.0	4.15	104	

a. The original content of UA found in real samples.

b. The extra added UA found in real samples.

References

18 J. Piedras, R. B. Dominguez and J. M. Gutiérrez, *Chemosensors*, 2021, **9,** 73.

51 M. Ramírez‐Berriozabal, L. Galicia, S. Gutiérrez‐Granados, J. S. Cortes and P. Herrasti, *Electroanal.*, 2008, **20**, 1678-1683.

52 C. Liao, C. Mak, M. Zhang, H. L. Chan and F. Yan, *Adv. Mater.*, 2015, **27**, 676-681.

53 J. Kim, S. Imani, W. R. de Araujo, J. Warchall, G. Valdés-Ramírez, T. R. Paixão, P. P. Mercier and J. Wang, *Biosens. Bioelectron.*, 2015, **74**, 1061-1068.

54 K. Ngamchuea, C. Batchelor-McAuley and R. G. Compton, *Sens. Actuators B Chem.*, 2018, **262**, 404-410.

55 W. Shi, J. Li, J. Wu, Q. Wei, C. Chen, N. Bao, C. Yu and H. Gu, *Anal. Bioanal. Chem.*, 2020, **412**, 7275-7283.

56 N. F. Azeredo, J. M. Gonçalves, P. O. Rossini, K. Araki, J. Wang and L. Angnes, *Microchim. Acta*, 2020, **187**, 1-11.

57 X. Huang, W. Shi, J. Li, N. Bao, C. Yu and H. Gu, *Anal. Chim. Acta*, 2020, **1103**, 75-83.

58 R. M. Cardoso, P. R. Silva, A. P. Lima, D. P. Rocha, T. C. Oliveira, T. M. do Prado, E. L. Fava, O. Fatibello-Filho, E. M. Richter and R. A. Munoz, *Sens. Actuators B Chem.*, 2020, **307**, 127621.

59 M. A. Bukharinova, N. Y. Stozhko, E. A. Novakovskaya, E. I. Khamzina, A. V. Tarasov and S. V. Sokolkov, *Biosensors*, 2021, **11**, 287.

60 G. Turkkan, S. Z. Bas, K. Atacan and M. Ozmen, *Anal. Methods*, 2022, **14**, 67-75.

61 J. Nong, N. Zhang, A. Wen and C. Hu, *J. Electroanal. Chem.*, 2024, **952**, 117982.